Blue Economy

Volume 2 | Issue 2 Article 2

2024

Integration of GPR and EMI Techniques for Engineering Applications in New Nubariya District, Egypt

Ali Abdalsalam
Department of Earth Science, Damanhour University, Damanhour, 22516, Egypt,
alialiabdalsalam@gmail.com

Osman Badran
Department of Earth Science, Damanhour University, Damanhour, 22516, Egypt

Elhamy A. Tarabees
Department of Earth Science, Damanhour University, Damanhour, 22516, Egypt

Abdellatif Younis
National Research Institute of Astronomy and Geophysics NRIAG, Helwan, 11421, Egypt

ISSN: 2805-2986 – e-ISSN: 2805-2994

RESEARCH ARTICLE

Integration of Ground Penetration Radar and Electromagnetic Induction Techniques for Engineering Applications in New Nubariya District, Egypt

Ali Abdalsalam [a,*], Osman Badran [a], Elhamy A. Tarabees [a], Abdellatif Younis [b]

[a] Department of Earth Science, Damanhour University, Damanhour, Egypt
[b] National Research Institute of Astronomy and Geophysics, Helwan, Egypt

Abstract

The Egyptian government has initiated an ambitious urban development initiative, encompassing the creation of new cities across different parts of the country. One significant project within this endeavor is the establishment of New Nubariya-2 city along the Wadi El Natrun, El Alamein Road, forming part of the broader framework of the New Nubariya district. Cavities in urban areas pose significant problems such as sinkholes and subsidence which can damage buildings, roads, and utility lines. To tackle these challenges, an integrated approach utilizing Ground Penetration Radar (GPR) and Electromagnetic Induction (EMI) surveys was employed to detect cavities effectively. This methodological fusion enhances the ability to identify potential hazards and mitigate risks within urban environments. The GPR survey utilizing a 100 MHz shielded antenna revealed hyperbolic curves indicative of reflections attributable to abnormal features due to man−maid activity (mining and crushing) along Road N1 and N2. The EMI survey conducted using the EM34-3 system in both horizontal dipole mode and vertical dipole mode highlighted predominantly high conductivity values throughout the study area, primarily attributed to the prevalence of clay material. Two distinct zones with significantly high conductivity values were evident in the northeastern and southeastern sectors. In the northeastern region, conductivity values peaked at 143 mS/m. These features may be aligned with the presence of gravel-crushing operations in the same area. In contrast, the southeastern region showed elevated conductivity values, indicating potential fracture zones. The results exhibit high accuracy in cavity detection using both GPR and EMI surveys.

Keywords: Cavities, Electromagnetic induction (EMI), Geophysical engineering, Ground penetration radar (GPR), New Nubariya

1. Introduction

Establishing the New Nubariya-2 city along the Wadi El Natrun, El Alamein Road, within the vast area of New Nubariya district, is a crucial project for Egyptian authorities. They aim to tackle the issues caused by overpopulation, particularly focusing on the West Nile Delta region. Cavities in urban areas pose significant problems, such as sinkholes and subsidence, which can damage buildings, roads, and utility lines. Geophysical detection of these cavities is challenging due to shallow depths and the need for precision, all compounded by construction site limitations and time constraints (Li *et al.*, 2008; Zhang *et al.*, 2020). Current research is designed to detect cavities by integrating the Ground Penetration Radar (GPR) and Electromagnetic Induction (EMI) methods. The GPR is well-suited for both detecting and mapping underground small or large voids or cavities (Kang *et al.*, 2019; Park *et al.*, 2019; Liu *et al.*,

Received 5 June 2024; revised 24 June 2024; accepted 24 June 2024.
Available online 25 July 2024

* Corresponding author at: Department of Earth Science, Damanhour University, Damanhour, 22516, Egypt.
E-mail address: alialiabdalsalam@gmail.com (A. Abdalsalam).

https://doi.org/10.57241/2805-2994.1026

2021; Mansour *et al.*, 2023). EMI, specifically the EM-34 instrument, has been used in detecting caves and mines (Santos *et al.*, 2001; Leucci and De Giorgi, 2005). However, their ability to pinpoint smaller targets is limited. So, the results demonstrate the high accuracy and complementary nature of GPR and EMI surveys in cavity detection, providing valuable insights into subsurface conditions and potential hazards within the urban environment.

In our study, we present a novel and comprehensive approach for cavity detection in urban areas, with a specific focus on New Nubariya-2 city. We conducted systematic surveys using GPR and EMI methods, targeting regions prone to cavity formation. GPR can offer high-resolution imaging to detect small and large voids, while EMI, particularly the EM34 instrument, will supplement by detecting larger underground features. Our aim is to enhance cavity detection accuracy and reliability by integrating these techniques. The correlation between discovered anomalies and geological parameters, facilitated by advanced data processing and interpretation, will assist in urban growth planning.

2. Material and methods

2.1. Study area

The research site, as depicted in Fig. 1, is situated west of the Nile Delta along the Wadi El Natrun, and El Alamein Road. It spans between latitudes 30°35′N and 30°40′N, and longitudes 29°48′E and, 29°53′E covering an approximate area of 50 km^2.

2.2. Geological settings

The geomorphology of the study area within Egypt's West Nile Delta region has been described by several authors, including (Sandford and Arkell, 1939; Said, 1962; Shata *et al.*, 1978; Embaby, 2003). This area is situated between two distinct geological features: Tableland and the El-Marbat depression. The Tableland is characterized by a flat to gently rolling landscape. This is due to the underlying layers of hard limestone that make up the formation. As a result of this geological composition, the topography gradually slopes downwards towards the north and east. In contrast, the El-Marbat depression formed through a different process. Tectonic subsidence caused the land to gradually sink below sea level. This subsidence was further amplified by the deposition of sediments transported by the Nile River, which deepened the depression over time.

From a geological standpoint, the study area, situated in the western sector of the Nile Delta, has been a subject of extensive research by renowned scholars such as (Sandford and Arkell, 1939; Said, 1962; Shata *et al.*, 1978). It is characterized by a diverse assemblage of geological formations originating from the Pliocene and Quaternary epochs, as depicted in Fig. 2. The Quaternary deposits of the

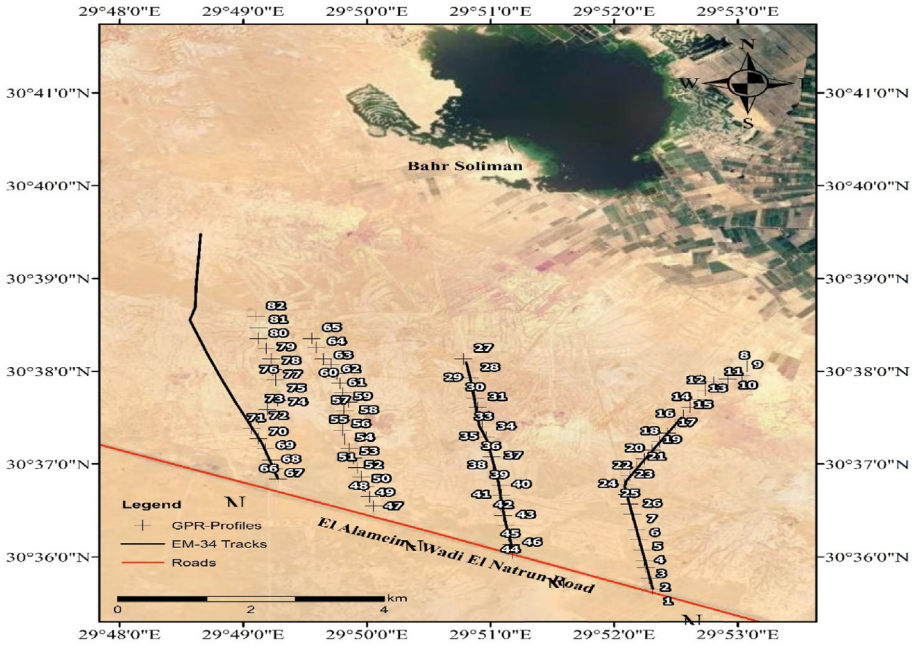

Fig. 1. Location map of the study area showing Ground Penetration Radar Profiles and EM-34 Tracks modified from (Google Earth Pro, 2024).

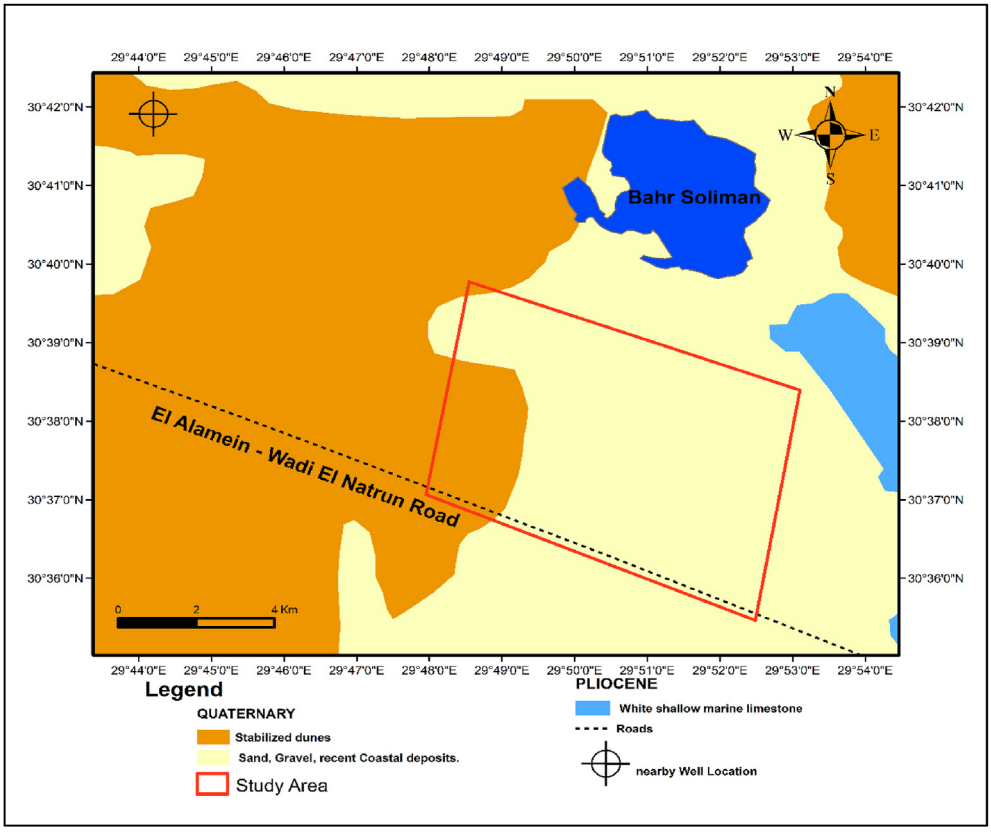

Fig. 2. Geological map of the area of study (CONOCO, 1987).

Nile Delta contain a mix of Holocene and Pleistocene sediments, including sand dunes, coastal deposits, sabkha deposits, and silty clay that form the Holocene strata. The Pleistocene segment is marked by alternating sands and clays, along with interbeds of limestone. The Pliocene sediments are distinguished by estuarine clayey facies at the base and fluvio-marine and shallow marine white limestones at the top, as documented by Salem and Osman (2016). In the subsurface geology, the western Nile Delta region unveils a significant sedimentary succession approximately 4000 m thick, spanning from Triassic to Pliocene times. This succession rests upon the Basement rocks dating back to the Precambrian Era, as indicated by data from the Sahara Wadi El Natrun test well, according to Salem and Osman (2017).

The nearby well in Fig. 2, drilled through a surface layer primarily composed of sand, clay, and gravel, encounters a subsurface sequence comprising predominantly clay, followed by a sand interspersed with clay and limestone. The water table is observed at a depth of 35 m. A clay-dominant stratigraphic sequence characterizes this sequence.

Structurally and tectonically, the study area falls within the unstable shelf that characterizes the western region of the Nile Delta, a prominent feature in the northern part of the Western Desert, as identified by Said (1962). This area is not just a simple geological structure but a complex system with three primary sets of lineaments comprising fractures and faults, each with distinct trends: N55°W–S55°E, N85°W–S85°E, and N75°E–S75°W, as documented by (El Shazly *et al.*, 1975). This intricate system, with its distinct lineaments and faults, presents a fascinating challenge for our understanding of the Earth's dynamics.

2.3. Ground penetrating radar (GPR)

It is a non-invasive geophysical technique with different possible configurations that can produce continuous profiles quickly and efficiently. The common-offset technique is the most used configuration for collecting the data by moving the radar systems consisting of a single transmitting and receiving antenna horizontally along a profile while maintaining a fixed separation distance between them (Neal, 2004). The impulse radar system is mostly used for road engineering purposes for easy data interpretation, this system operates by transmitting a very short pulse with a fixed central

high-frequency range from 1 MHz to 1000 MHz, toward the target using one or multiple antennas, the system records the signals back-reflected by dielectric discontinuities in the subsurface. The two-way travel time signals are captured in the time domain to create detailed maps of reflections, enabling valuable insights into the internal composition and condition of roads (Benedetto *et al.*, 2017). It detects electrical discontinuities in a shallow subsurface (Bernatek-Jakiel and Kondracka, 2019). The electromagnetic wave propagates in the air at the speed of light (0.3 m/ns) by sending a pulse into the subsurface its velocity v is reduced since it is dependent on the relative dielectric permittivity ϵ, the magnetic permeability μ and the electric conductivity σ. Mathematically it is defined as:

$$v = \frac{C}{\sqrt{\epsilon\mu \frac{1+\sqrt{1+\left(1+\frac{\sigma}{2\pi f\epsilon}\right)}}{2}}} \quad (1)$$

In nonmagnetic ($\mu = 1$) low-loss materials, such as clean sand and gravel ($\frac{\sigma}{2\pi f} \approx 0$). The velocity of electromagnetic waves is reduced to the expression:

$$v = \frac{c}{\sqrt{\epsilon}} \quad (2)$$

Equations (1 and 2) show that the velocity of electromagnetic waves propagating on the ground is decreased compared with the velocity in the air (Neal, 2004). In the propagation of electromagnetic waves through a medium, velocity and attenuation are critical factors. When waves traverse conductive materials, energy loss occurs as heat due to electric currents, known as attenuation. This loss reduces radar wave penetration depth, affecting detection capabilities (Peña *et al.*, 2023). Underground cavities, due to their distinct dielectric properties compared with surrounding soil, generate strong electromagnetic reflections. GPR is thus the best method for detecting these cavities beneath urban roads (Liu *et al.*, 2021).

2.4. Electromagnetic induction (EMI)

EMI relies on Faraday's law and is employed to detect conductive material beneath the surface in a noninvasive manner (Martini *et al.*, 2017; Pradipta,*et al.*, 2022). Its rapid measurement and high sensitivity are derived from the induction principle which eliminates the need for direct contact with the ground (Peña *et al.*, 2023). The basic principles, as in Fig. 3. When an alternating current is applied to the transmitter coil (T), it

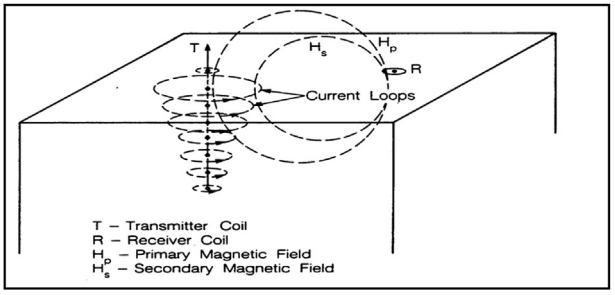

Fig. 3. Simplified diagram illustrating the principles of electromagnetic induction and ground conductivity measurements (Goldstein et al., 1988).

generates a time-varying magnetic field (H_P). This magnetic field induces eddy currents in the earth, which weaken as they penetrate deeper. However, these eddy currents give rise to secondary magnetic fields (H_S), these secondary fields, along with the primary field (H_P) are detected by a receiver coil (R) situated at a known distance from the transmitter (Goldstein *et al.*, 1988). The strength of these secondary fields is a function of ground conductivity, frequency of the current, and transmitter-receiver separation (McNeill, 1980). Differences in intensity, direction, and phase among electromagnetic fields can serve as indicators for detecting the presence of conductive bodies. The EM 34-3 conductivity meter measures the conductivity as it is directly proportional to the secondary to primary magnetic field ratio, as the equation. If the operating frequency and separation are known, the terrain conductivity can be easily determined.

$$\sigma_a = \frac{4H_S}{\omega\mu_0 S^2 H_P}$$

where H_S = the secondary magnetic field, H_P = the primary magnetic field, σ_a = apparent ground conductivity (S/m), μ_0 = permeability of free space, S = intercoil spacing (m), $\omega = 2\ \pi$ f, f = frequency (cycles/sec). Electrical conductivity fluctuates based on various factors such as soil or rock type, porosity, permeability, degree of saturation, and the electrochemical properties of liquids present in the pores (McNeill, 1980).

2.5. Data acquisition

2.5.1. GPR data acquisition

The paper utilizes a MALA GPR with a shielded antenna, operating at a precise lower frequency of 100 MHz. This meticulous choice ensures an optimal penetration depth, striking a balance between enhanced vertical resolution and reduced penetration depth associated with higher frequencies. In the

study, a total of 82 GPR profiles Fig. 1, each spanning 200 m, were meticulously conducted within a time window of 400 and 450 ns along designated roads with distances ranging from 3500 to 5000 m labeled N1, N2, N3, and N4. These specific roads were selected based on identifying prevalent issues within the area under investigation. This approach guarantees comprehensive coverage of the targeted area while upholding scientific rigor in data collection and analysis.

2.5.2. EMI data acquisition

The Geonics EM34-3 conductivity meter played a pivotal role in our data acquisition process. This system, with its two primary modes, the Horizontal Dipole Mode (HDM) and Vertical Dipole Mode (VDM), demonstrated its versatility and precision. HDM and VDM. In HDM, both the transmitter and receiver coils are oriented vertically, while in VDM, both coils are placed horizontally on the surface. The data acquisition was taken along tracks N1, N2, and N4. The figure involved using the Geonics EM34-3 conductivity meter with intercoil spacing of 10 m, with measurements taken at 20 m intervals, and both HDM and VDM were employed. Additionally, data was acquired using intercoil spacing of 20 m, with measurements taken at 20 m intervals, but only VDM was used. McNeill (1980) proposed utilizing 0.75 times the intercoil spacing for the (HDM) and 1.5 times the intercoil spacing for the (VDM). The VDM offers double the exploration depth compared with the HDM and demonstrates greater sensitivity to lateral conductivity variations. Nevertheless, it is essential to acknowledge that coil misalignment significantly affects the reliability of the VDM. Varied intercoil spacing and operating modes enable imaging ground conductivity distribution with depth, enhancing geophysical exploration of geological features.

2.6. Data processing

2.6.1. GPR

Reflex software was utilized to process GPR data, using a license granted by Damanhur University. We perform straightforward processing steps in raw data, avoiding overprocessing because more complicated processing methods may introduce bias and artifacts into the data (Cassidy, 2009). Processing steps involved in data processing (Cassidy, 2009; Robinson *et al.*, 2013; Kalenda *et al.*, 2017; Gomes *et al.*, 2022; Nanda *et al.*, 2024) include:

(a) Static correction of zero-time: adjusts data for near-surface irregularities.
(b) Dewow filtering: removes low-frequency noise.
(c) Gain processing: amplifies signal strength and attenuates noise.
(d) Background removal: eliminates unwanted ambient noise.
(e) Time-depth conversion: converts travel times to depth measurements using the hyperbole overlap approach yielded a propagation velocity of 0.11 m/ns.
(f) FK-migration: transforms data for subsurface structure visualization.

2.6.2. EMI

EMI data Fig. 4 was processed using Python code to generate conductivity contouring maps in millisiemens per meter (mS/m), each corresponding to different depths: HDM with intercoil spacing of 10 m at 7.5 m depth, VDM with intercoil spacing of 10 m at 15 m depth, and VDM with intercoil spacing of 20 m at 30 m depth (Figs. 7–9).

3. Results

3.1. GPR

The results of the ground penetrating radar (GPR) survey (Figs. 5 and 6) conducted with a 100 MHz antenna, utilizing a time window of 400–450 ns, revealed distinct hyperbolic curves indicative of reflections attributable to abnormal features due to man–maid activity (mining and crushing) along Road N1 situated at depths of 1.5 and 1.9 m Fig. 5 (profile 15). And along Road N2 is situated at a depth of 2.7 m Fig. 6 (profile 29). Conversely, profiles acquired along N3, N4, and other sections exhibited an absence of such subsurface anomalies.

3.2. EMI

The EM 34-3 systems are highly adept at detecting sizable underground voids such as caves and mine workings. However, their ability to pinpoint smaller targets is somewhat limited. Our analysis of the EM survey data is presented through contoured conductivity maps in millisiemens per meter (mS/m), each corresponding to different depths. Specifically, the depth maps include HDM with an intercoil spacing of 10 m at a depth of 7.5 m, VDM with an intercoil spacing of 10 m at a depth of 15 m, and VDM with an intercoil spacing of 20 m at a depth of 30 m (Figs. 7–9).

4. Discussion

The GPR data revealed hyperbolic curves indicative of reflections attributable to abnormal features

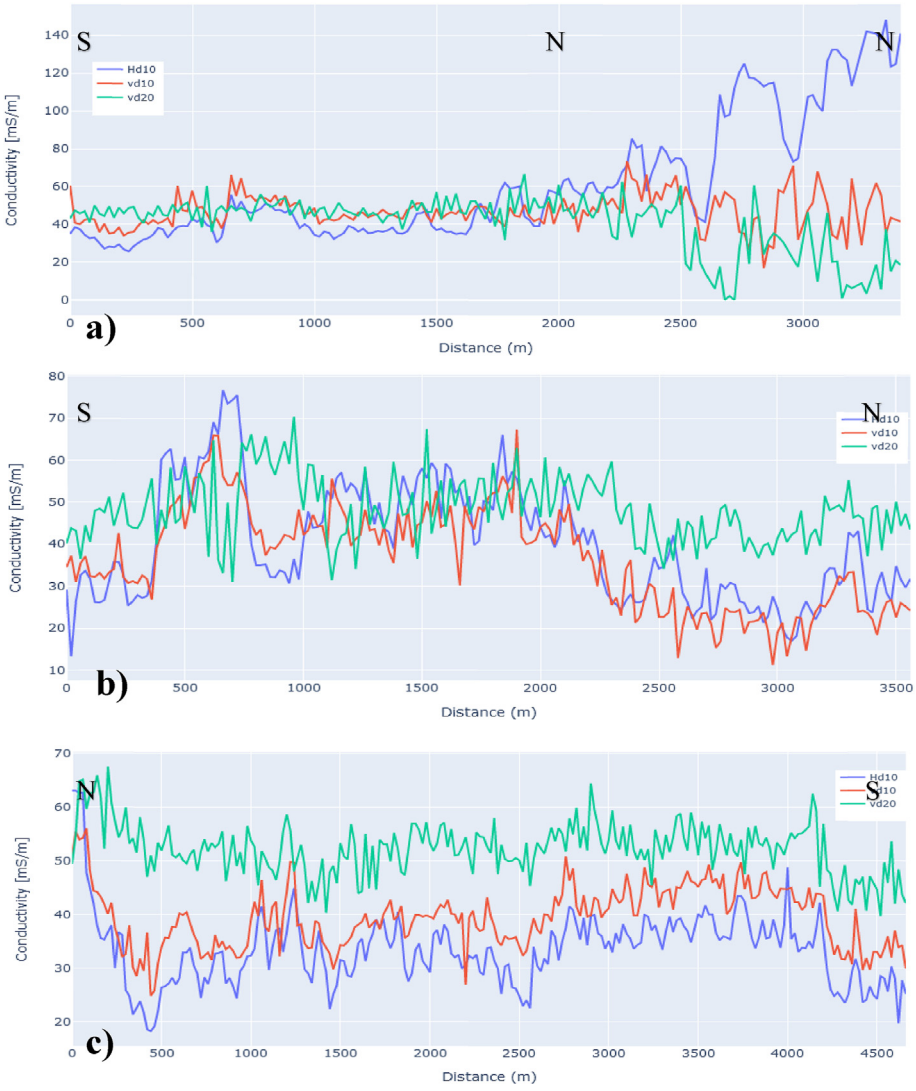

Fig. 4. Electromagnetic induction data Plot a) at road N1, b) at road N2, c) at road N4.

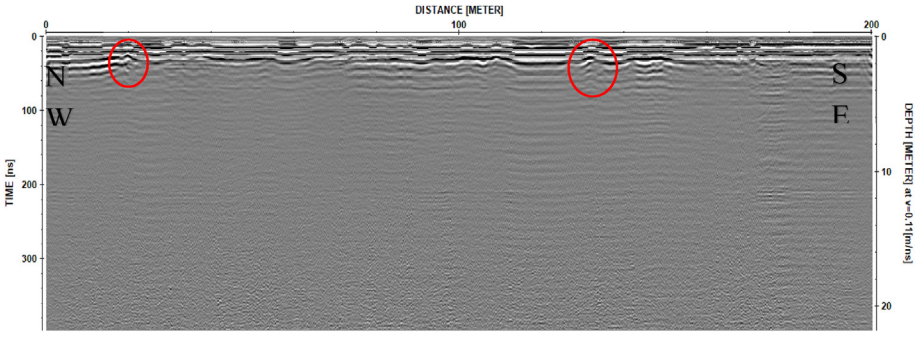

Fig. 5. The two dimensional ground penetrating radar profile (100 MHz antenna with 400 ns time windows) along Road N1 at selected profiles 15. The red circles show hyperbolic curves indicating reflections caused by abnormal features.

due to man–maid activity (mining and crushing) along Road N1 and N2 which does not affect the construction when removing the surface part of the soil.

The EM apparent conductivity measurement maps portray predominantly high conductivity values, primarily attributed to the prevalence of clay material (Davis and Annan, 1989; Casas *et al.*, 2019;

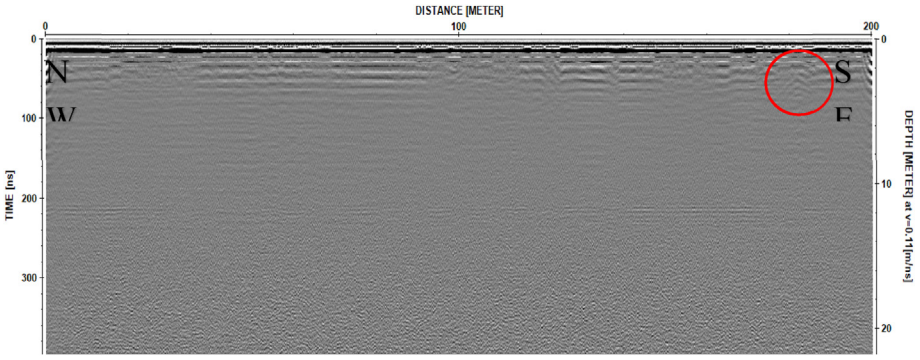

Fig. 6. The two dimensional ground penetrating radar profile (100 MHz antenna with 400 ns time windows (along Road N2 at selected profiles 29. The red circle shows hyperbolic curves indicating reflections caused by abnormal features.

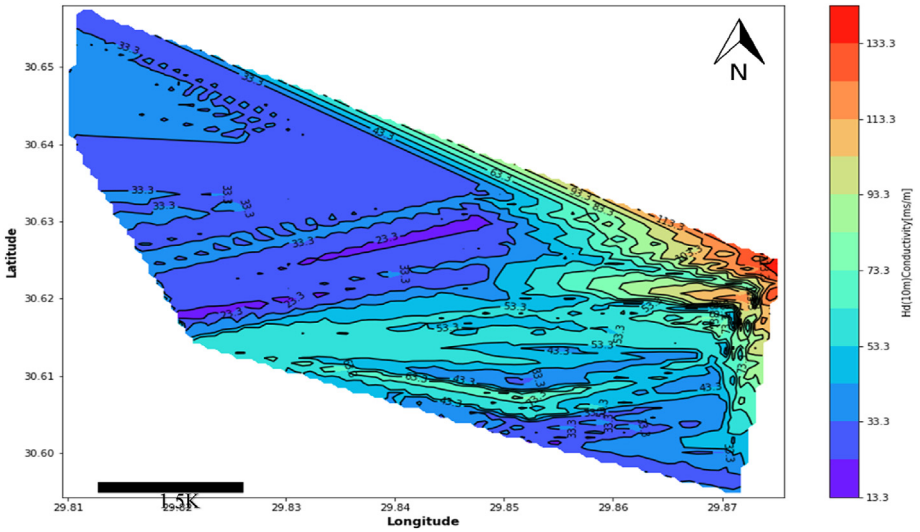

Fig. 7. Map of the apparent conductivity in the study area, with a horizontal dipole mode (HDM) with an intercoil spacing of 10 m at a depth of 7.5 m.

Peña *et al.*, 2023). Additionally, two distinct zones with significantly high conductivity values are present in the northeastern and southeastern sectors of the study area.

In the northeastern region, high conductivity values reaching up to 143 mS/m are observed in Figs. 7 and 8. This feature may be attributed to man-made effects as the northeastern region has been subjected to drilling activities for rock gravel crusher operations exposing the area. The presence of crushed gravel can influence conductivity, with the hydraulic conductivity of crushed materials like gravel being highly dependent on factors such as particle size, distribution, and the presence of infilling materials such as sand, silt, or clay (Woessner and Poeter, 2020). If the crushed gravel area is filled with a conductive material (like water or certain types of minerals), it could result in higher conductivity readings.

As depth increases, conductivity values gradually diminish, ultimately close to zero at a depth of 30 m Fig. 9. The decrease in conductivity with depth could be due to the increased closure of fractures with depth due to the increasing normal stress from the weight of the overlying rock (AquaResource Inc, 2007).

In the southeastern region, elevated conductivity values are evident in all three maps, indicating the potential presence of conductive materials or geological structures favorable to fluid movement. The contour patterns observed suggest the existence of fracture zones. Fractured zones are known to exhibit heightened conductivity attributed to the infiltration of water or other conductive substances within the fractures (Powers *et al.*, 1999).

The western sector in all three maps has lower conductivity (more Resistance) compared with the other sectors which makes it more suitable for construction than others.

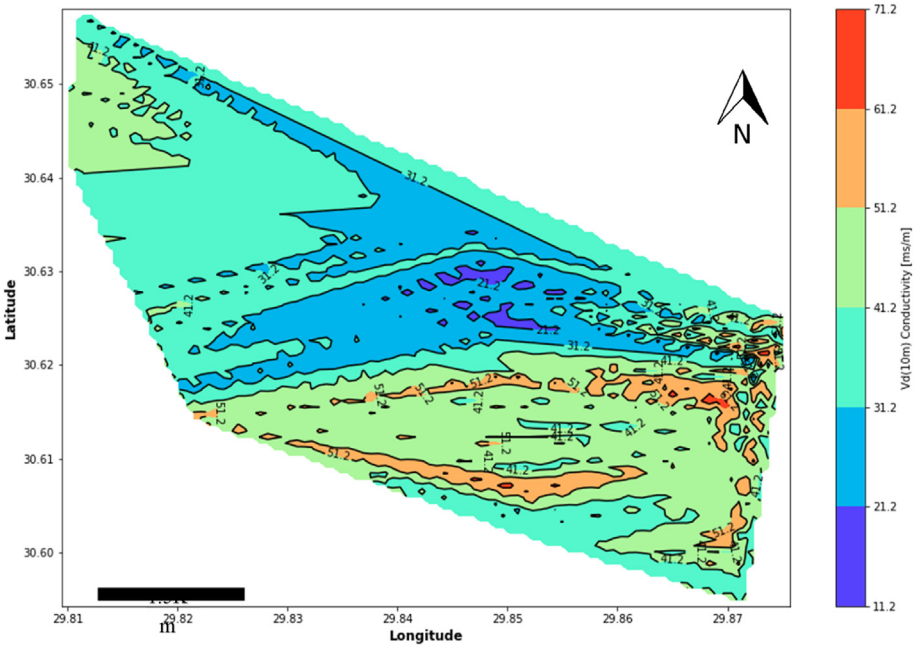

Fig. 8. Map of the apparent conductivity in the study area, with a vertical dipole mode (VDM) with an intercoil spacing of 10 m at a depth of 15 m.

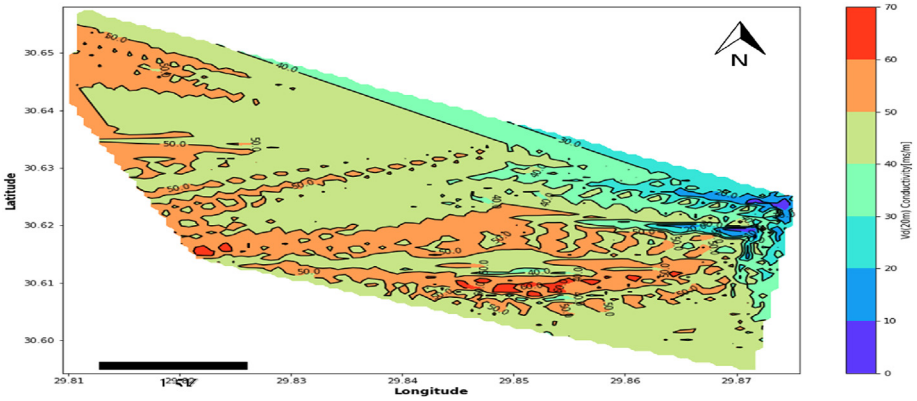

Fig. 9. Map of the apparent conductivity in the study area, with a vertical dipole mode (VDM) with an intercoil spacing of 20 m at a depth of 30 m.

4.1. Conclusion

The primary focus of this work is to detect cavities within the urban area of New Nubariya-2, which pose significant risks such as sinkholes and subsidence, potentially causing damage to buildings, roads, and utility lines. The integration of GPR and EMI surveys proved highly effective in detecting subsurface cavities within the study area.

The GPR survey utilizing a 100 MHz shielded antenna revealed hyperbolic curves indicative of reflections attributable to abnormal features due to man–maid activity (mining and crushing) along Road N1 and N2.

The EMI survey conducted using the EM34-3 system revealed predominantly high conductivity values throughout the area, attributed to clay material, with two distinct zones of significantly high conductivity observed in the northeastern and southeastern. The increasing conductivity in the northeastern aligns with the presence of gravel-crushing operations in the same area. In the southeastern region, the contour patterns observed suggest the existence of fracture zones. The lower conductivity (more Resistance) of the western sector in the study area compared with the other sectors makes it more suitable for construction.

Overall, the results demonstrate the high accuracy and complementary nature of GPR and EMI surveys in cavity detection, providing valuable insights into subsurface conditions and potential hazards within the urban environment.

Funding

There were no primary funders for this research.

Declaration of interest statement

The authors of this manuscript declare that there are no conflicts of interest regarding the publication of this work.

References

AquaResource Inc, 2007. SSFL Hydraulic Conductivity vs. Depth Relation. Int J Rock Mech. www.dtsc-ssfl.com/files/lib_rcra_groundwater/3d_report/3dreport/REPORT/AppdxG-Conductivity-Depth.pdf.

Benedetto, A., Tosti, F., Ciampoli, L.B., D'Amico, F., 2017. An overview of ground-penetrating radar signal processing techniques for road inspections. Signal Process. 132, 201–209.

Bernatek-Jakiel, A., Kondracka, M., 2019. Detection of Soil Pipes Using Ground Penetrating Radar. Rem. Sens. 11, 1864.

Casas, A., Castanyer, P., Himi, M., Lovera, R., Rivero, L., Santos, M., et al., 2019. Effectiveness of electromagnetic conductivity mapping for delineating subsurface structures related to the Roman port of Emporiae. In: 2019 IMEKO TC-4 International Conference on Metrology for Archaeology and Cultural Heritage. IMEKO, Florence, Italy, pp. 259–264.

Cassidy, N.J., 2009. Ground Penetrating Radar Data Processing, Modelling and Analysis. Elsevier eBooks, pp. 141–176.

CONOCO, 1987. Geological Maps of Egypt Scale 1:500,000. Sheet Nos. NG 36 NW Cairo. The Egyptian General Petroleum Corporation, Egypt.

Davis, J.L., Annan, A.P., 1989. Ground-penetrating radar for high-resolution mapping of soil and rock stratigraphy 1. Geophys. Prospect. 37, 531–551.

El Shazly, E.M., Abdel Hady, M.A., El Ghawaby, M.A., El Kassas, I.A., El Khawasik, S.M., El Shazly, M.M., Sanad, S., 1975. Geological Interpretation of Landsat Satellite Images for West Nile Delta Area, Egypt. Remote Sensing Research Project, Academy of Scientific Research and Technology, Egypt, p. 86.

Embaby, A., 2003. Environmental Evaluation for Geomorphological Situation of the Water and Soil Resources of the Region North of the Sadat City, West Nile Delta, Egypt.

Goldstein, N., Alumbaugh, D., Benson, S., 1988. Ground conductivity measurements adjacent to the kesterson ponds 1,2, and 5. Available at: https://escholarship.org/uc/item/46z599t9.

Gomes, K.J.M., Oliva, P.A.C., Da Rocha, H.O., De Alcântara Mendes, R., Da Costa, A.C.G., Miranda, C.D.S., De Oliveira Almeida, N., 2022. Evaluation of the contamination of the subsurface and groundwater by monoaromatic hydrocarbons in an eastern Amazonian town in northern Brazil. Environ. Earth Sci. 82, 1.

Google Earth Pro, 2024. Location Map of the Study Area Showing GPR Profiles and EM-34 Tracks. Available at: https://www.google.com/earth/.

Kalenda, P., Tengler, R., Sebela, S., 2017. Detection of unknown caves, influx into Planinska jama. ZRC SAZU Karst Research Institute. https://doi.org/10.13140/RG.2.2.26556.54409. Available at:

Kang, M.-S., Kim, N., Im, S.B., Lee, J.-J., An, Y.-K., 2019. 3D GPR Image-based UcNet for Enhancing Underground Cavity Detectability. Rem. Sens. 11, 2545.

Leucci, G., De Giorgi, L., 2005. Integrated geophysical surveys to assess the structural conditions of a karstic cave of archaeological importance. Nat. Hazards Earth Syst. Sci. 5, 17–22.

Li, X.J., Dou, S.E., Qu, H., 2008. A view on application and development of engineering geophysical prospecting and testing in city. Chin. J. Eng. Geophys. 5, 564–573.

Liu, H., Shi, Z., Li, J., Liu, C., Meng, X., Du, Y., Chen, J., 2021. Detection of road cavities in urban cities by 3D ground-penetrating radar. Geophysics 86, WA25–WA33.

Mansour, K., ABD, M., Hafiz, M., Ebrahim, S.M., Gomaa, M., Salem, M., 2023. Detection for severe caves and sinkholes in non-clastic rock type using GPR technique. NRIAG J Astrono Geophys 12, 121–131.

Martini, E., Werban, U., Zacharias, S., Pohle, M., Dietrich, P., Wollschläger, U., 2017. Repeated electromagnetic induction measurements for mapping soil moisture at the field scale: validation with data from a wireless soil moisture monitoring network. Hydrol. Earth Syst. Sci. 21, 495–513.

McNeill, J.D., 1980. Electromagnetic Terrain Conductivity Measurement at Low Induction Numbers. Geonics Ltd. Technical Note TN-6. Available at: https://www.scirp.org/reference/referencespapers?referenceid=1203516.

Neal, A., 2004. Ground-penetrating radar and its use in sedimentology: principles, problems, and progress. Earth Sci. Rev. 66, 261–330.

Nanda, M., Ismail, N., Mahlia, M., Amril, F., Munir, B., Asyqari, A., et al., 2024. Application of ground-penetrating radar for shallow subsurface investigation at the coastal area of lhok village, lhoong, aceh besar regency, aceh. BIO Web of Conferences 87, 2015.

Park, J.-J., Chung, Y., Hong, G., 2019. A Method for Cavity Scale Estimation Based on Ground-Penetrating Radar (GPR) Explorations: An Experimental Study. Adv. Civ. Eng. 2019, 1–13.

Peña, R., Oliva, P.A.C., Abrunhosa, F.A., 2023. Application of the Ground Penetrating Radar (GPR) and Electromagnetic (EM34-3) Geophysical Tools and Sedimentology for the Evaluation of the Subsurface of Sites Earmarked for Aquaculture Ponds in the Amazon Region of Northern Brazil. Appl. Sci. 13, 11107.

Powers, C.J., Singha, K., Haeni, F.P., 1999. Integration of surface geophysical methods for fracture detection in bedrock at Mirror Lake, New Hampshire. In: Proceedings of Technical Meeting of US Geological Toxic Substances Hydrology Program, Charleston, South Carolina. USGS Water-Resources Investigations Report, pp. 757–768.

Pradipta, A., Soupios, P., Kourgialas, N.N., Doula, M., Dokou, Z., Makkawi, M., et al., 2022. Remote Sensing, Geophysics, and Modeling to Support Precision Agriculture—Part 1: Soil Applications. Water 14, 1158.

Robinson, M., Bristow, C.S., Mckinley, J., Ruffell, A., 2013. Ground Penetrating Radar. ResearchGate. Available at: https://www.researchgate.net/publication/291293516_Ground_Penetrating_Radar.

Said, R., 1962. The Geology of Egypt. Google Books. Elsevier Publishing Company.

Salem, Z.E.-S., Osman, O.M., 2016. Use of major ions to evaluate the hydrogeochemistry of groundwater influenced by reclamation and seawater intrusion, West Nile Delta, Egypt. Environ. Sci. Pollut. Res. 24, 3675–3704.

Salem, Z.E., Osman, O.M., 2017. Use of Geoelectrical Resistivity to Delineate the Seawater Intrusion in the Northwestern Part of the Nile Delta, Egypt. Handb. Environ. Chem. 73, 425–459. Available at: https://doi.org/10.1007/698_2017_175.

Sandford, K.S., Arkell, W.J., 1939. Paleolithic Man and Nile Valley in Lower Egypt. Oriental Institute Publications, Chicago, IL.

Santos, F.A.M., Matias, H., Goncalves, R., 2001. The use of EM343 surveys in cave detection. Eur. J. Environ. Eng. Geophys. 6, 153–166.

Shata, A.A., El Shazly, M.M., Attia, S.H., Aboul-Fetouh, M., 1978. The geology of the quaternary deposits and their natural relation to soil formations in the fringes west of the Nile Delta, Egypt. Desert Inst Bull, ARE 28, 43–77.

Woessner, W.W., Poeter, E.P., 2020. Hydrogeologic Properties of Earth Materials and Principles of Groundwater Flow. The Groundwater Project.

Zhang, J., Liu, S., Yang, C., Liu, X., Wang, B., 2020. Detection of urban underground cavities using seismic scattered waves: a case study along the Xuzhou Metro Line 1 in China. Near Surf. Geophys. 19, 95–107.